THE ASTROPHYSICAL JOURNAL, 445:840–854, 1995 June 1


# A STUDY OF CORONAL X-RAY EMISSION FROM SHORT-PERIOD ALGOL BINARIES

K. P. SINGH,[1,2,3] S. A. DRAKE,[1,4,5] AND N. E. WHITE[1,6]

*Received 1994 October 3; accepted 1994 December 7*


## ABSTRACT

A study of X-ray emission from five short-period Algol-type binaries based on observations with *ASCA* and *ROSAT* is presented. We have observed RZ Cas with both satellites, and $\beta$ Per, U Cep, $\delta$ Lib, and TW Dra with *ROSAT*. Significant intensity variations are seen in the X-ray emission from RZ Cas, U Cep, TW Dra, and $\delta$ Lib. These variations seem unrelated to the eclipsing behavior of these systems and are probably due to either rotational modulation of compact active regions on the surfaces of the chromospherically active secondary components or to flaring activity in the systems. The spectra of all but one of the systems require the presence of at least two discrete plasma components with different temperatures (0.6–0.7 keV, and $\sim$2 keV) and the abundances of the medium-$Z$ elements 20%–50% of the solar photospheric values. The high resolving power and signal-to-noise ratio of the *ASCA* spectra allow us to individually constrain the coronal abundances of O, Ne, Mg, Si, S, and Fe in RZ Cas. We demonstrate that, if we use the elemental abundances and temperatures obtained from the analysis of their *ASCA* spectra as (fixed) inputs, to fit the *ROSAT* PSPC spectra well requires the presence of a third component ($kT \sim 0.2$–$0.3$ keV) in RZ Cas and $\beta$ Per. A continuous emission measure model of the power-law type [$\mathrm{EM}(T) \propto (T/T_{\max})^{\alpha}$] generally gives a poor fit to the *ASCA* and *ROSAT* data on most sources. Circumstellar or circumbinary absorbing matter seems to be present in some of these systems, as indicated by the variable total column density needed to fit their X-ray spectra.


*Subject headings:* binaries: eclipsing — circumstellar matter — stars: coronae — X-rays: stars

## 1. INTRODUCTION

Algol-type binary systems, named after the prototype Algol (hereafter $\beta$ Per to avoid confusion), are eclipsing binaries that typically contain an early-type (B5–A5) main-sequence primary accreting matter from a less massive late-type (G–K) subgiant secondary that fills its critical equipotential volume ("Roche lobe"). The hot primary star is almost always smaller than the cool star and is eclipsed periodically, resulting in a deep minimum in the optical light curves (the primary eclipse). The secondary star in Algols is often found to be chromospherically active, i.e., it has a corona which is a source of X-ray and radio emission, and also shows starspot activity in the near-infrared, and thus resembles the active secondary stars in the RS CVn binaries (Hall 1989). The X-ray luminosities of Algols are indeed very similar to those of the RS CVn binaries (White & Marshall 1983). Prior to the X-ray observatory *ASCA* (*Advanced Satellite for Cosmology and Astrophysics*), however, only $\beta$ Per itself had been observed with high enough spectral resolution and signal-to-noise ratio in the X-ray region so as to obtain detailed information on its coronal plasma (Swank et al. 1981; White et al. 1986; Stern et al. 1992; Smale et al. 1995). The results of an *ASCA* observation of $\beta$ Per have also recently been presented (Antunes, Nagase, & White 1994). These studies have revealed that the X-ray emission from $\beta$ Per requires at least two plasma components with temperatures of $\sim$0.7 keV and $\sim$2.5 keV, and Antunes et al. (1994) have further found evidence for elemental abundances a factor of 2–3 below the solar photospheric values for a number of the elements.

We have carried out an X-ray spectral study of five Algol-type binaries, viz., $\beta$ Per, RZ Cas, U Cep, $\delta$ Lib, and TW Dra. These objects are known X-ray sources (White & Marshall 1983; McCluskey & Kondo 1984), but no X-ray spectra have ever been reported for the last four objects named above. The main properties of these binary systems are listed in Table 1. These objects are all short-period Algols (i.e., they have orbital periods less than 5 days). Optical observations of $\beta$ Per and other short-period Algol systems have sometimes found evidence for the presence of circumstellar (or circumbinary) material with transient characteristics (see Richards 1993 and references therein), raising the possibility that X-ray spectroscopy of these systems might also reveal variable absorption column densities. Two of these systems, viz., $\beta$ Per and RZ Cas, were targeted for high-resolution studies with *ASCA* in the 0.5–10 keV energy range. All of them were observed with *ROSAT* for the purpose of obtaining low-energy (0.1–2.4 keV) high-sensitivity spectra (but with much lower spectral resolution than *ASCA*, of course). The *ROSAT* spectra complement the *ASCA* spectra in these two cases but were not, it should be noted, taken simultaneously or even contemporaneously. The preliminary results from the *ASCA* observations of $\beta$ Per have already been presented (Antunes et al. 1994). Here, we present a detailed analysis of the *ASCA* observations of RZ Cas and of the *ROSAT* observations of all five Algols.

The paper is organized as follows. In § 2 we present the details of observations, followed by the analysis and results in § 3. A discussion of all results follows in § 4 before a summary of conclusions in § 5.

[1] Code 668, Laboratory for High Energy Astrophysics, NASA/GSFC, Greenbelt, MD 20771.
[2] NRC-NASA Senior Research Associate, on leave from Tata Institute of Fundamental Research, Bombay, India.
[3] kps@rosserv.gsfc.nasa.gov.
[4] Also USRA, Code 610.3, NASA/GSFC.
[5] drake@lheavx.gsfc.nasa.gov.
[6] white@heagip.gsfc.nasa.gov.

TABLE 1

PROPERTIES OF SELECTED ALGOL-TYPE BINARIES

| Properties | $\beta$ Per | RZ Cas | U Cep | $\delta$ Lib | TW Dra |
|---|---|---|---|---|---|
| Spectral Types | B8 V + K2 IV | A3 V + K3 IV | B7 V + G4 IV | A0 V + K2 IV | A6 V + K0 IV |
| Masses ($M_\odot$) | $3.7 \pm 0.3$ | $2.205 \pm 0.075$ | $4.2 \pm 0.2$ | $4.9 \pm 0.2$ | 1.7 |
| | $0.81 \pm 0.05$ | $0.73 \pm 0.02$ | $2.8 \pm 0.8$ | $1.7 \pm 0.2$ | 0.8 |
| Radii ($R_\odot$) | $3.1 \pm 0.1$ | $1.67 \pm 0.03$ | $2.8 \pm 0.2$ | 4.1 | 2.4 |
| | $3.4 \pm 0.1$ | $1.94 \pm 0.03$ | $4.9 \pm 0.2$ | 4.2 | 3.4 |
| Distance (pc) | 31 | 73 | 170 | 75 | 190 |
| log $L_{bol}$ (ergs s$^{-1}$) | 35.78 | 34.62 | 35.88 | 35.67 | 34.89 |
| | 34.22 | 33.72 | 34.98 | 34.48 | 34.47 |
| log $L_x$[a] (ergs s$^{-1}$) | 30.97 | 30.36 to 31.18 | 31.11 | 30.64 | 30.67 |
| Orbital Period (days) | 2.8673285 | 1.195254 | 2.493041 | 2.3274 | 2.8069 |
| Epoch (HJD) for Eclipse Minimum | 2,441,773.4894[b] | 2,448,581.3155[c] | 2,445,937.7272[d] | 2,422,852.3598 | 2,433,888.452 |
| | | 2,449,031.9273[c] | | | |
| Orbital Inclination (degrees) | 81.4 | 83.3 | 83–90 | $78.6 \pm 0.2$ | 90 |
| Rotational Velocity $v \sin i$ (km s$^{-1}$) | 53 | 81 | 310 | 76 | 50 |
| Starspot Activity[e]/Photometric Changes | Yes | ? | Yes | ? | ? |

[a] Present observations in the 0.2–2.4 keV energy range.
[b] Kim 1989.
[c] Narusawa et al. 1994.
[d] Faulkner 1986.
[e] See Richards & Albright 1993.
NOTE.—Properties are from (i) the SIMBAD database, (ii) Giuricin et al. 1983, and (iii) Tomkin 1978.

## 2. OBSERVATIONS

### 2.1. *ASCA*

RZ Cas was observed with *ASCA* on 1994 February 5 from 05:48 UT to 18:34 UT as part of the guest observer program. The *ASCA* observatory (for details, see Tanaka et al. 1994), contains four imaging thin-foil grazing incidence X-ray telescopes, two of which are equipped with solid state imaging spectrometers (SIS) and the other two with gas imaging spectrometers (GIS). Each SIS consists of four CCD chips and each GIS is a gas scintillation proportional counter. The SIS cameras were operated in the 2-CCD mode for these observations with a resultant field of view of 22.'2 × 11.'2 and a time resolution of 8 s. The energy resolution of both SIS is about 2% (FWHM) at 5.9 keV, degrading to 6% at 1.0 keV. The GIS data were taken with a time resolution of 62.5 ms. Each GIS has a circular field of view with 20′ radius. The energy resolution of GIS is about 7.8% (FWHM) at 5.9 keV and 19% at 1.0 keV. The energy bandwidth for >10% efficiency is 0.5–10 keV for the SIS and 0.8–10 keV for the GIS.

The data were selected by applying different criteria for the SIS and the GIS, since the SIS is sensitive to light leakage from Earth. For the SIS, the data were selected when the telescope viewing direction was >25° from the bright Earth limb and >10° from the dark Earth, while the GIS data were selected for the periods from the dark Earth, while the GIS data were selected for the periods when the Earth elevation angle was >10°. These selections resulted in useful exposure times of ~13,000 s and ~12,000 s in the SIS and GIS detectors, respectively. Hot and flickering pixels in the CCDs were eliminated by rejecting those pixels that did not follow Poissonian statistics (see Day et al. 1994 for details). The counts and pulse height spectra were accumulated from a source region of 4′ radius in the SIS and 6′ radius in the GIS, while the background was taken from source-free regions in the SIS and GIS where counts from the outer wings of the point-spread function of the source were minimized. Typical count rates were 0.16 counts s$^{-1}$ (SIS) and 0.06 counts s$^{-1}$ (GIS).

### 2.2. *ROSAT*

The five Algol-type binaries listed in Table 1 were observed as a part of the *ROSAT* guest observer program. The observations were done with the *ROSAT* X-ray telescope and a position sensitive proportional counter (PSPC) as the detector (Truemper 1983; Pfeffermann et al. 1987). The PSPC has an energy resolution ($\Delta E/E$) of $\simeq$0.42 at 1 keV and a bandwidth of 0.1–2.4 keV. The spectral resolution is quite moderate when compared with that of the *ASCA* detectors, but the energy range is more sensitive to the presence of low-energy absorption and soft emission components, and has a considerable overlap with that of *ASCA*. The details of the observations are given in Table 2. The exposure times, the observed count rates, and the binary phases at the start and end of the observation based on the ephemeris given in Table 1 are also listed here. Observations of U Cep were centered on the secondary eclipse. $\beta$ Per, RZ Cas, and TW Dra observations were "near" the primary eclipse in these systems but did not cover the eclipse. The source counts were selected from a typical radius of about 3.'5 (4.'0 for high source intensity). The background was accumulated from several neighboring regions. These observations resulted in very high quality spectra with an excellent signal-to-noise ratio for all the sources observed, except TW Dra for which only 720 counts were accumulated.

## 3. ANALYSIS AND RESULTS

### 3.1. *X-Ray Fluxes and Luminosities*

The 0.2–2.4 keV X-ray fluxes from the *ROSAT* PSPC observations based on the best-fit two-component model (see § 3.3) are given in Table 2 for all the objects, and their corresponding X-ray luminosities are given in Table 1. The X-ray flux detected from RZ Cas with *ASCA* in the energy range of 0.4–5.0 keV is $4.0 \times 10^{-12}$ ergs cm$^{-2}$ s$^{-1}$, which is comparable to the value detected in its "low" state (see § 3.2.1) with the PSPC. We have compared these values given in Table 2 with the earlier measurements using the IPC in the corresponding energy range. The uncertainty in the IPC flux values due to the

TABLE 2

DETAILS OF *ROSAT* PSPC OBSERVATIONS

| NAME | DATE | | | | | BINARY PHASE | EXPOSURE TIME (s) | MEAN COUNT RATE AND FLUX[a,b] | TOTAL COUNTS[a] |
|---|---|---|---|---|---|---|---|---|---|
| | Start/End | Year | Month | Day | UT | | | | |
| $\beta$ Per ..... | Start | 1992 | 01 | 30 | 19:14 | 0.032 | 4670 | 9.508 ± 0.005 | 44400 |
| | End | 1992 | 01 | 30 | 22:51 | 0.08 | | (8.2) | |
| RZ Cas..... | Start | 1991 | 09 | 09 | 17:45 | 0.70 | 11290 | 0.58 to 2.90 ± 0.02 | 2015 (L)[c] |
| | End | 1991 | 09 | 10 | 13:22 | 1.38 | | (0.46 to 2.382) | 22670 (H) |
| | Start | 1992 | 02 | 05 | 09:18 | 0.0632 | 2500 | 1.08 ± 0.02 | 2700 |
| | End | 1992 | 02 | 05 | 20:50 | 0.47 | | (0.97) | |
| U Cep..... | Start | 1991 | 09 | 16 | 15:30 | 0.2775 | 32350 | 0.415 ± 0.004 | 13425 |
| | End | 1991 | 09 | 17 | 14:39 | 0.625 | | (0.37) | |
| $\delta$ Lib ..... | Start | 1992 | 01 | 25 | 02:39 | 0.866 | 14710 | 0.632 ± 0.007 | 9296 |
| | End | 1992 | 01 | 30 | 09:21 | 3.13 | | (0.65) | |
| TW Dra..... | Start | 1992 | 02 | 28 | 07:26 | 0.9986 | 5810 | 0.124 ± 0.005 | 720 |
| | End | 1992 | 02 | 29 | 10.58 | 1.407 | | (0.107) | |

[a] For PH channels 17–248 corresponding to 0.2–2.4 keV.
[b] X-ray flux is in parentheses in units of $10^{-11}$ ergs cm$^{-2}$ s$^{-1}$.
[c] L and H refer to "low" and "high" states of RZ Cas.

lack of determination of spectral parameters with the IPC and uncertainty of the IPC gain is about 20% (see Tananbaum et al. 1979). The X-ray flux detected from RZ Cas in the *ASCA* observations is comparable (within ~30%) to the value detected with the IPC by McCluskey & Kondo (1984) about 12 yr ago. On the other hand, U Cep was ~3 times brighter during the PSPC observations as compared to the IPC observations (White & Marshall 1983). TW Dra had a similar X-ray flux in the PSPC compared to the IPC observation, whereas $\delta$ Lib was ~2 times brighter during the PSPC observations. $\beta$ Per was nearly twice as bright in our PSPC observation than during the IPC observations. The similarity of the observed brightness form $\beta$ Per with another PSPC observation 6 months later is discussed below (see § 3.2.3).

### 3.2. *The X-Ray Light Curves*

We have searched for time variability in the source counts, and found the sources to be either strongly or marginally variable in almost all the observations. Two of the strongest variabilities were seen in the *ASCA* and *ROSAT* observations of RZ Cas and in the *ROSAT* observations of U Cep.

#### 3.2.1. *RZ Cas*

In Figure 1*a* we show the light curve of RZ Cas as observed with SIS0 and SIS1 in two energy bands viz., 0.4–1.0 keV and 1.0–5.0 keV. The counts from both the detectors have been combined and binned every 512 s. A sharp increase by a factor of 2 in intensity in the hard channels is visible at about 16:30 UT. The increase in the softer channels, however, appears to be more gradual. The hardness ratio, defined as the ratio of the counts in the 1.0–5.0 keV energy range to the counts in the 0.4–1.0 keV energy range, is nearly the same during the high count rate and the low count rate states (i.e., after and before the transition). The background level, which is negligible here, is shown as the dash-dot lines.

The 0.1–2.4 keV X-ray curve of RZ Cas during the *ROSAT* observations is shown in Figure 1*b*. The data have been binned every 256 s. The count rate is found to increase by a factor of ~5 after a 6 hr gap in the observation and then decreased by a factor of ~3 in a follow-up observation about 6 months later. Henceforth, we will designate the three stages of RZ Cas in the *ROSAT* observations as the "low," "high," and "mid-" intensity stages. To study spectral variations associated with the intensity changes, we define two hardness ratios—(i) a high-energy hardness ratio (HR1) as the ratio of counts in the 1.0–2.4 keV divided by the counts in the 0.4–1.0 keV energy range, and (ii) a low-energy hardness ratio (HR2) defined as the ratio of counts in the 0.4–1.0 keV divided by the counts in the 0.1–0.4 keV energy range. The background was subtracted from the source intensities before taking the ratios. The data were binned every 1024 s. These hardness ratios are plotted as a function of total intensity in Figure 1*c*. The hardness ratio variation is also shown in a color-color plot in Figure 1*d*, where the highest intensity points are in the top left-hand corner. Figures 1*c* and 1*d* show that, as the intensity increases, the very hard channels and the very soft channels show a more marked increase than the medium-energy channels. The implications of this result will be discussed in § 4.

The binary phases during the observations are also shown in Figures 1*a*, and 1*b*, and 1*c*. The eclipse of the hot primary star by the cool secondary defines the phase 0.0 and is known as the primary eclipse. The secondary eclipse, where the cool secondary star is eclipsed by the primary, is at phase 0.5. The duration of the eclipses is about ±0.1 in phase around the minima (Narusawa, Nakamura, & Yamasaki 1994). The present observations of RZ Cas do not cover the eclipse durations very well, and the observed variations in the X-ray intensity in Figures 1*a*–1*c* do not appear to be related to either the primary or the secondary eclipse in the X-rays.

#### 3.2.2. *U Cep*

In Figure 2 we show the X-ray count rates in the energy band 0.4–2.4 keV and the high-energy hardness ratio (HR1) as observed from U Cep with the PSPC. The data were binned every 4096 s. The intensity is observed to fall off almost linearly for roughly the first half of the observation whereas the hardness ratio, HR1, remains constant during this time. The hardness ratio, HR1, is somewhat higher for the lowest intensity points (henceforth, referred to as "hard" state) towards the end of the observations. The early part of the light curve is referred to as the "soft" state of U Cep. To see if the increase in HR1 is caused by an increase in the absorption, we examined the low-

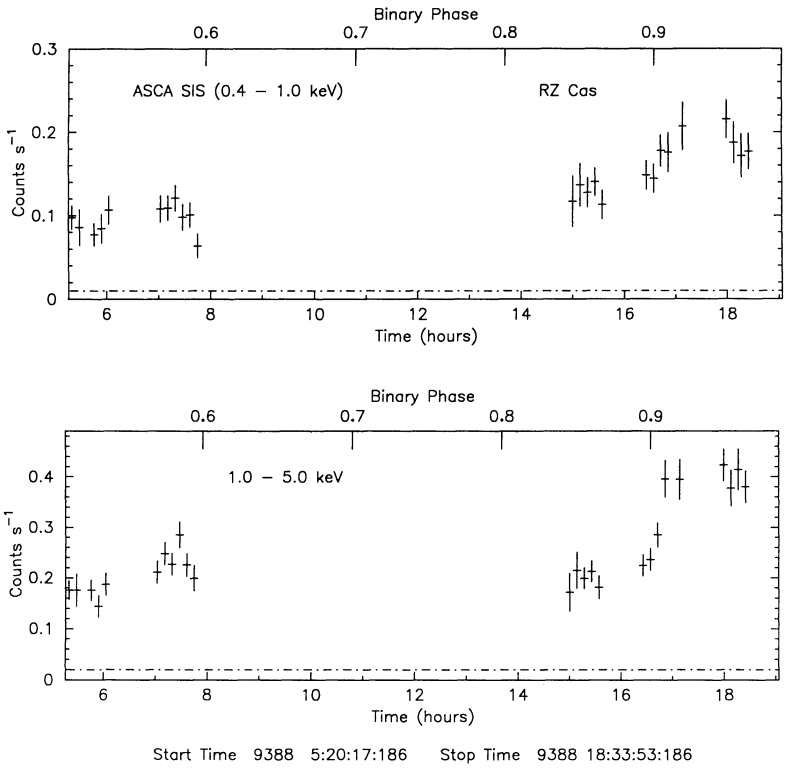


FIG. 1*a*

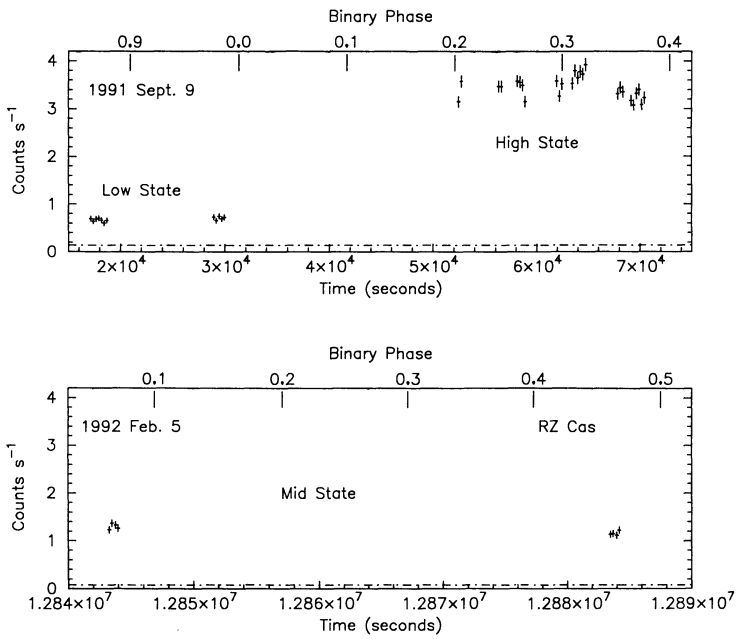


FIG. 1*b*

FIG. 1.—(*a*) X-ray light curve of RZ Cas in two energy bands as observed with the *ASCA*. Count rates from both SIS0 and SIS1 have been summed in a bin size of 512 s. The start and stop times indicated are for MJD 40000+. The binary phases are marked on the top of the *X*-axis. The dash-dotted line shows the background level. (*b*) Background-subtracted 0.1–2.4 keV X-ray light curve of RZ Cas as observed with the *ROSAT* PSPC. The counts have been binned every 256 s. The dash-dotted line shows the background level. (*c*) The hardness ratios HR1 and HR2, as defined in the text, are plotted as a function of the total intensity observed with the *ROSAT* PSPC. The background-subtracted data were binned every 1024 s before taking the ratios. (*d*) Color-color plot of RZ Cas based on (*c*).

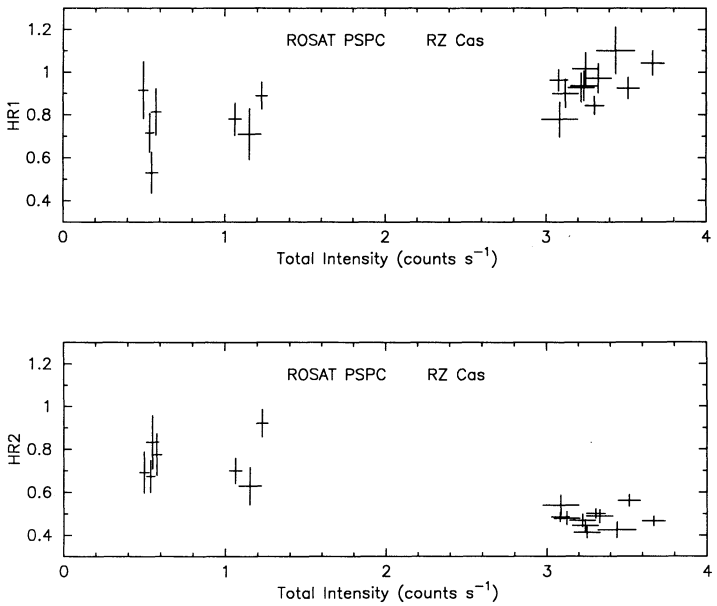


FIG. 1*c*

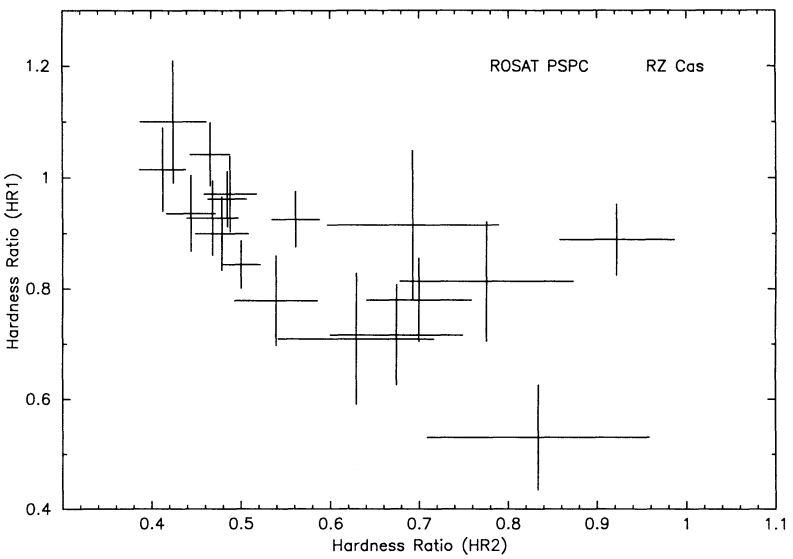


FIG. 1*d*

energy hardness ratio (HR2) but found no evidence for variation. Although the sampling of the light curve is not very good there is some indication of a dip near the binary phase of 0.5 and may be related to the secondary eclipse. A longer and more sensitive observation is needed to verify this behavior.

#### 3.2.3. *β Per*

$\beta$ Per was observed during the binary phase of 0.03 to 0.08, a region not covered in the *ASCA* observations (Antunes et al. 1994) and coarsely sampled in the *ROSAT* observations 6 months later (Ottmann 1994). The source appears to be about as bright as during the binary phases 0.6–0.9 and equal in intensity to the high intensity observed at phase 0.057 in *ROSAT* observations 6 months later (Ottmann 1994).

### 3.3. *Spectral Analysis*

#### 3.3.1. *Spectral Models*

We have used the XSPEC (Version 8.41) spectral analysis package to fit the data with two different spectral models for thermal-equilibrium plasmas, viz. the Raymond & Smith or RS model (Raymond 1990; Raymond & Smith 1978), and the Mewe-Kaastra or "meka" model (Mewe, Gronenschild, & van den Oord 1985; Kaastra 1992). Except for a small difference in the derived temperatures, the two spectral models give similar results. The results presented here are based on "meka" model for ease of comparison with our earlier work on active stars where we also found somewhat better fits using "meka" model (Drake et al. 1994). We tried (a) single-

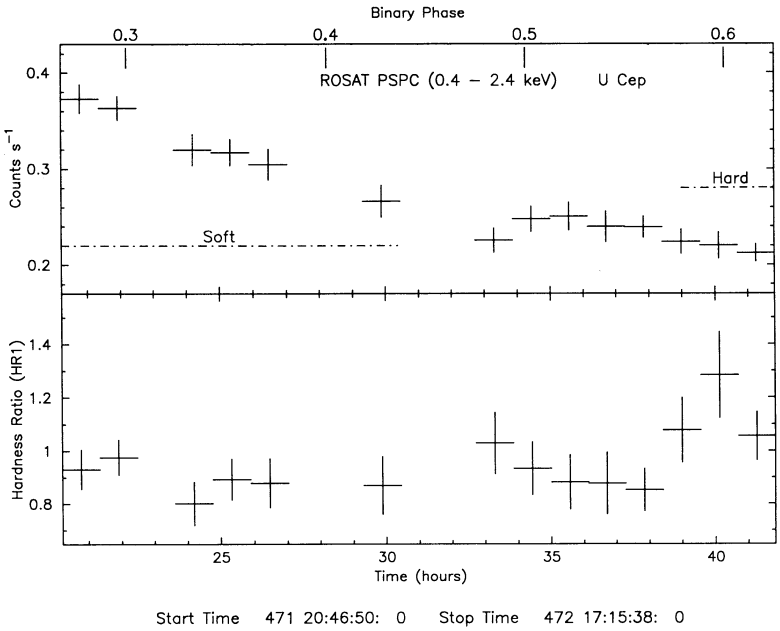


FIG. 2.—X-ray light curve of U Cep as observed with the *ROSAT* PSPC in the 0.4–2.4 keV energy band and the hardness ratio variations in U Cep. The counts were binned every 4096 s.

temperature or isothermal plasma models, (b) a model consisting of two or more discrete plasma components at different temperatures, and (c) a plasma model with continuous emission measure (CEM) distribution which is a power-law function of the temperature of the type, $\mathrm{EM}(T) \propto (T/T_{\max})^{\alpha}$, where $T_{\max}$ is the maximum temperature of the plasma and $\alpha$ is the slope of the emission measure (EM) distribution (Schmitt et al. 1990). The last of these is a good approximation to models that have been used to describe the EM distribution of individual coronal loops on the Sun (Vesecky, Antiochos, & Underwood 1979; Antiochos & Noci 1986). It has been used to fit the X-ray emission from stellar coronae which would normally involve an ensemble of such loops (Stern, Antiochos, & Harnden 1986; Schmitt et al. 1990; Dempsey et al. 1993b). We have kept $\alpha$ and $T_{\max}$ as free parameters. The elemental abundances in the plasma for all of these different models, were varied with respect to the solar photospheric values taken from Anders & Grevesse (1989). We also tried models having EM distribution as a Gaussian function of temperature.

### 3.3.2. *ASCA Spectra of RZ Cas*

The X-ray spectra of RZ Cas as obtained from the two SIS and two GIS detectors onboard *ASCA* are shown in Figures 3*a* and 3*b*, respectively. The data were binned so that there were at least 16 counts per bin. We used the latest SIS and GIS response matrices released on 1994 June 30 and carried out a joint fit to the data from the four detectors. The *ASCA* detectors are not sensitive to absorption below a level of a few times $10^{19}$ cm$^{-2}$, values which may be present in these nearby stellar systems due to interstellar and circumstellar matter. Higher values of $10^{20}$ cm$^{-2}$ or more can influence the derived abundances of N and O. Therefore, the value of the equivalent hydrogen column density, $N_{\mathrm{H}}$, was kept fixed at $10^{19}$ cm$^{-2}$ for fitting the *ASCA* spectra. The validity of this assumption was subsequently justified when the PSPC spectra (§ 3.3.3) extending to lower energy X-rays showed only a small absorption to be present in RZ Cas in its different intensity states. We find that single-temperature plasma models, assuming either solar photospheric (Anders & Grevesse 1989) or nonsolar abundances, are unsatisfactory, as they yield unacceptably large values of the fit statistic $\chi^2$. The "meka" plasma models that have two discrete components at different temperatures and with solar photospheric abundances can yield acceptable fits ($\chi^2 = 252.3$ for 231 degrees of freedom, or the reduced $\chi^2$ statistic, $\chi^2_{\nu} = 1.1$). A considerable improvement in the fit (a reduction in the $\chi^2$, $\Delta\chi^2 = 31.4$) is obtained, however, when the abundances of all the elements (other than H) are allowed to vary by a common factor relative to their solar values. The best-fit value for the abundances of all the elements ($Z > 1$) is found to be $0.26^{+0.11}_{-0.08}$ times the solar value. A similar improvement ($\Delta\chi^2 = 36.0$) also results when the abundances of the elements N, O, Ne, Mg, Si, S, and Fe are allowed to vary. The abundances for the other elements, He, C, Na, Al, Ar, Ca, and Ni, are insensitive to variations and were kept fixed at their solar photospheric values. The abundances for the two temperature components were assumed to be the same. The best-fit model in this case has $\chi^2_{\nu} = 0.97$. The improvement resulting from allowing nonsolar abundances is significant at $>99.9\%$ level based on the $F$-statistic. The best-fit model for the variable abundance model is shown as a histogram in the top panels of Figures 3*a* and 3*b*. In the bottom panel of the figures we show the $\chi^2$ for the residuals, in the sense of (observed − calculated) × $\chi^2$.

The best-fit values and 90% uncertainties of the parameters of the two-component plasma emission model are listed in Table 3. The abundances listed here are with respect to the values given by Anders & Grevesse (1989). Notice that Grevesse, Noels, & Sauval (1992) have suggested a revision of the solar photospheric abundances for certain elements: to place our derived values on this revised scale, the abundances listed in Tables 3 and 4 for N, O, Ne, and Fe should be multiplied by factors of 1.2, 1.148, 1.025, and 1.444, respectively. For example, in the case of RZ Cas the abundance of Fe in Table 3 would become $0.38^{+0.20}_{-0.14}$ of the solar photospheric value. An

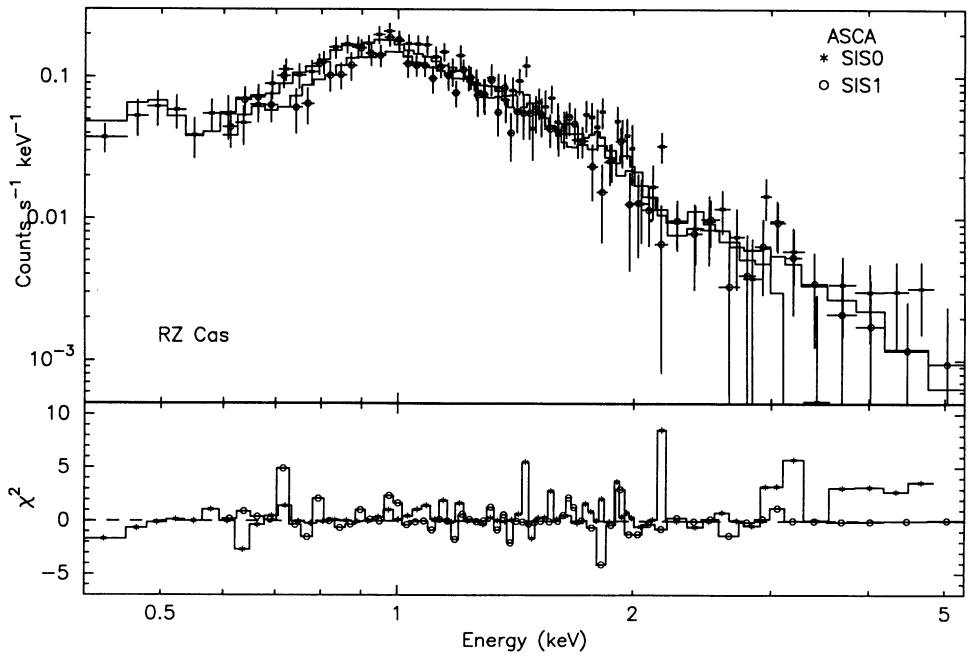


FIG. 3*a*

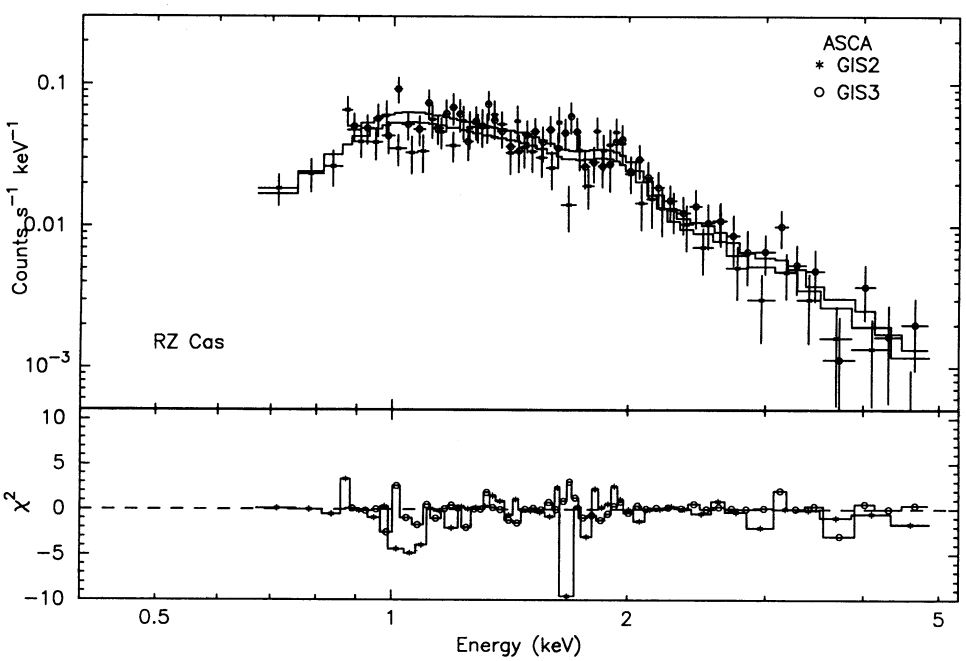


FIG. 3*b*

FIG. 3.—(*a*) X-ray spectra of RZ Cas as observed with the CCD detectors aboard *ASCA*. The best-fit two-component model jointly fitted to the SIS and GIS spectra are shown as histograms. The lower panel shows the contribution of the residuals to the $\chi^2$. (*b*) Same as in (*a*) for GIS2 and GIS3 detectors aboard *ASCA*.

additional complication is that the heavy element abundances derived in this analysis are, in general, highly correlated with the abundance of Fe, as has been pointed out earlier by Drake et al. (1994): in other words, their abundances relative to Fe are more robust than their abundances relative to H. Nevertheless, the face-value results of our two-component modeling of the *ASCA* spectrum of RZ Cas are that the abundances of the elements O, Ne, Mg, Si, S and Fe relative to H are 2–4 times lower than their solar photospheric values. The remaining elements have inferred abundances that are consistent with solar values (see Table 3). The significance of these deviations from solar abundance values has been evaluated by finding the $\Delta\chi^2$ for a solar value for an element versus its best-fit value, while keeping all the other parameters in the Table 3 free. Using the

TABLE 3

SPECTRAL RESULTS FOR RZ CAS AND THEIR COMPARISON WITH $\beta$ PER

A. TWO-TEMPERATURE FITS TO ALL FOUR *ASCA* DETECTORS

| Parameter | RZ Cas[a] | $\beta$ Per[b] |
|---|---|---|
| $kT_1$ (keV) | $2.0^{+0.4}_{-0.3}$ | 2.36–2.70 |
| $EM_1(10^{53}$ cm$^{-3})$ | $1.45^{+0.3}_{-0.3}$ | 3.2–5.8 |
| $kT_2$ (keV) | $0.70^{+0.04}_{-0.05}$ | 0.64 |
| $EM_2(10^{53}$ cm$^{-3})$ | $1.3^{+0.5}_{-0.4}$ | 1.7–3.4 |

B. ELEMENTAL ABUNDANCES RELATIVE TO SOLAR PHOTOSPHERIC

| Element | RZ Cas | $\beta$ Per |
|---|---|---|
| N | 0.0 (<2.5) | <0.1 |
| O | $0.24^{+0.26}_{-0.20}$ | 0.24 ± 0.03 |
| Ne | 0.0 (<0.51) | 1.08 ± 0.07 |
| Mg | $0.31^{+0.32}_{-0.25}$ | 0.47 ± 0.04 |
| Si | $0.52^{+0.28}_{-0.22}$ | 0.47 ± 0.03 |
| S | 0.25 (<0.83) | 0.09 ± 0.04 |
| Fe | $0.26^{+0.14}_{-0.10}$ | 0.32 ± 0.01 |
| $\chi^2_\nu$ | 0.97 | 1.30 |

NOTE.—$N_H$ was kept fixed at $10^{19}$ cm$^{-2}$.
[a] Present study. Errors are with 90% confidence based on $\chi^2_{min} + 2.71$.
[b] From Antunes et al. 1994.

*F*-statistic, we find that the nonsolar abundances for O, Ne, Mg, Si, S, and Fe with $\Delta\chi^2$ values of 13, 10.4, 9.8, 8.1, 7.0, and 23.0 respectively, are significant at >99% confidence level.

The CEM plasma models give poorer fits to the data compared to those found for the two-component plasma fits, as they resulted in fits of $\chi^2_\nu = 1.49$ for the solar photospheric abundances, and $\chi^2_\nu = 1.03$ for the variable elemental abundances. Since the latter is statistically acceptable, however, we list the best-fit parameters for this model in Table 4. It can be seen that the abundances thus derived are also generally subsolar, and quite similar (considering the uncertainties and with the exception of Ne) to the values shown in Table 3 for the two-component model. A comparison of the residuals from this best-fit model with the residuals from the two-component variable abundance "meka" model shows that the differences in the two models are mostly (*a*) in the region where the Ne and Fe L-shell lines contribute strongly leading to a different estimate for the Ne abundance in the two models, and (*b*) in the region below 0.55 keV.

TABLE 4

SPECTRAL RESULTS FOR RZ CAS BASED ON CEM MODEL

A. SIMULTANEOUS FIT TO ALL FOUR *ASCA* DETECTORS

| Parameter | Value |
|---|---|
| $kT_{max}$ (keV) | $2.17^{+0.04}_{-0.05}$ |
| Slope ($\alpha$) | $2.24^{+0.30}_{-0.20}$ |

B. ELEMENTAL ABUNDANCES RELATIVE TO SOLAR PHOTOSPHERIC

| Element | Abundance |
|---|---|
| N | 0.0 (<2.0) |
| O | $0.12^{+0.16}_{-0.12}$ |
| Ne | $0.74^{+0.34}_{-0.30}$ |
| Mg | $0.35^{+0.34}_{-0.30}$ |
| Si | $0.50^{+0.25}_{-0.21}$ |
| S | $0.28^{+0.38}_{-0.28}$ |
| Fe | $0.19^{+0.08}_{-0.06}$ |
| $\chi^2_\nu$ | 1.03 |

NOTE.—$N_H$ was kept fixed at $10^{19}$ cm$^{-2}$.
[a] Errors are with 90% confidence based on $\chi^2_{min} + 2.71$.

We also find that a three-temperature component model with temperatures of 0.17 ± 0.06 keV, 0.70 ± 0.03 keV, and 2.6 ± 0.3 keV, and with solar photospheric abundances gives an acceptable fit to the data ($\chi^2_\nu = 1.06$). The fact that either a model with discrete temperature components (2T with variable abundances or 3T with solar photospheric abundances) or a CEM model can fit the *ASCA* spectra of RZ Cas fairly well indicates that we do not have sufficient information in these spectra to severely constrain the temperature distribution of the corona of this binary. In Figure 4, we plot the EM as a function of temperature ($T$) for the competing models in the case of RZ Cas. The solar photospheric abundance models have a steeper distribution of EM as compared to the better fitted subsolar abundance models. For example, in the two-temperature models the effect of nonsolar abundances is to decrease the highest temperature and to increase the emission measure of the lower temperature component; similarly in the CEM models the emission measure increases more at the low temperatures than at the high temperatures. This is mainly due to the fitting procedure that tries to compensate for excess line emission at low energies from the low-temperature component in the solar abundance models. We have also tried models where the EM is distributed as a Gaussian function, keeping the width of the Gaussian as one of the free parameters. The best fits with such models require two components having the same peak temperatures as in the case of two discrete (delta function) components and having very narrow widths: $\sigma = 0.02$ keV for the low-$T$ component and 0.06 keV for the high-$T$ component. This again shows the preference for either two discrete or very narrow components in the EM distribution. These narrow widths are depicted in Figure 4.

### 3.3.3. *PSPC Spectra: Independent Analysis*

The *ROSAT* PSPC data were grouped every eight pulse height channels and then fitted. We used the most appropriate PSPC response matrix available: *pspcb_92mar11.rmf* for observations performed before 1991 October 11, and *pspcb_93jan12.rmf* for observations after that date (Turner & George 1994). Due to some calibration uncertainties in the response function of the PSPC at very low energies, we have ignored the data in the first 16 pulse height channels and thus we fitted the data above 0.18 keV only. These X-ray spectra were fitted with the plasma models in the same manner as the *ASCA* data (see above). In this case, the $N_H$ value was allowed to vary. Three X-ray spectra were separately accumulated for the three different intensity states of RZ Cas and fitted separately. The spectra of all the sources were fitted poorly by a single-temperature component plasma with solar photospheric abundances. Such models were, therefore, rejected due to the unacceptably high value of $\chi^2_\nu$ ($\simeq$5.0–63) for all the sources except TW Dra (the lowest signal-to-noise ratio spectrum), for which $\chi^2_\nu$ is 1.23. The plasma models with two components at different temperatures but with solar photospheric abundances

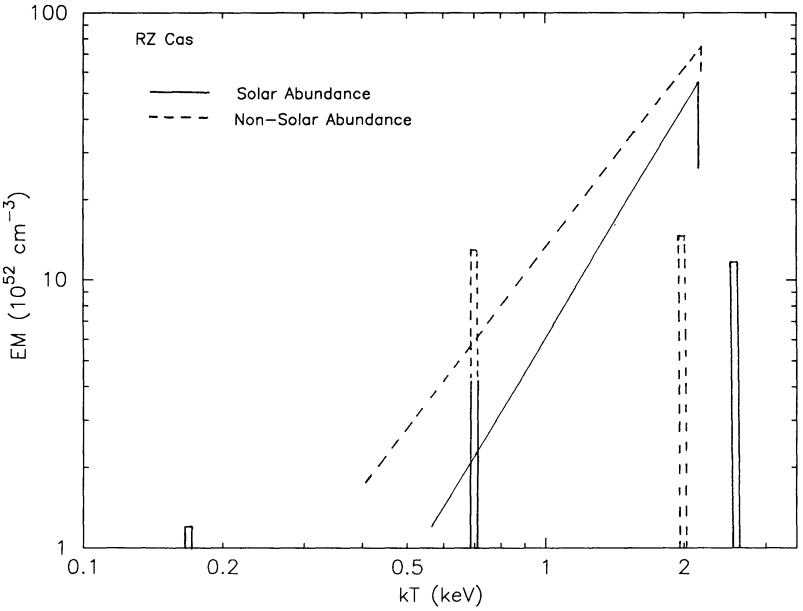


FIG. 4.—Emission measure distribution as a function of temperature for different spectral models fitted to the *ASCA* spectra of RZ Cas. Only relative distribution of EMs is shown. The width of the discrete components is only indicative.

also appear to be inadequate for $\beta$ Per ($\chi^2_\nu = 9.0$), RZ Cas ($\chi^2_\nu = 4.0$ and 2.2 for the high and low state, respectively), and for U Cep ($\chi^2_\nu = 1.93$). The signal-to-noise ratio in the spectra of TW Dra, and to some extent $\delta$ Lib and RZ Cas (mid-state), is not as good as for the other observations, and therefore, we cannot constrain the models strongly in these cases. Single-temperature plasma models with variable abundances were also rejected ($\chi^2_\nu > 2.0$) for $\beta$ Per, U Cep and RZ Cas (high state). Since the energy resolution of the PSPC is not adequate for resolving the contribution of individual elements to the plasma emission, the abundances of all the elements were varied together.

The best fits were obtained with the "meka" plasma models with two components at different temperatures and with non-solar abundances. The best-fit values and 90% uncertainties of the parameters of the two-component plasma emission model are listed in Table 5. There is an excellent agreement with the results from the *ASCA* analysis. The best-fit models to the PSPC spectra of the five Algol binaries require abundances that are between one-fifth and one-half of the solar photospheric values. The temperatures for the two plasma components are completely consistent with those inferred from the analysis of the *ASCA* spectra of $\beta$ Per and RZ Cas. Also notice that the independent analysis of the PSPC has resulted in emission measures (EMs) of the two plasma components which are comparable to those obtained from the *ASCA* spectra. The small differences are due probably to the intrinsic variability of the X-ray emission and nonsimultaneity of the observations.

In the case of RZ Cas we find that the high-temperature plasma component dominates during the high-intensity state due to an enormous increase in its emission measure. The values of the low temperature, $N_H$, and the abundance factor are also somewhat different in the "low" and "high" states of RZ Cas. The very small value for $N_H$, the higher elemental abundance, and the lower value of the low-temperature component are all indicative of an excess at very low energies in the "high" state. This is consistent with the trends seen in Figures 1*c* and 1*d* which showed that HR1 increased and HR2 decreased in going from the "low" to "high" state. The X-ray spectra and the best-fit two-component spectral models are shown in Figure 5 for $\beta$ Per and RZ Cas (high, mid-, and low states), Figure 6 for U Cep (soft and hard states), and in Figure

TABLE 5

SPECTRAL RESULTS: TWO-TEMPERATURE FITS TO PSPC DATA

| | | RZ Cas | | | | | |
|---|---|---|---|---|---|---|---|
| PARAMETER | $\beta$ PER | LOW | HIGH | MID | U CEP | $\delta$ LIB | TW DRA[a] |
| $kT_1$ (keV) | $0.68 \pm 0.02$ | $0.57^{+0.09}_{-0.12}$ | $0.42^{+0.09}_{-0.07}$ | $0.62^{+0.09}_{-0.11}$ | $0.65^{+0.07}_{-0.12}$ | $0.70 \pm 0.05$ | $0.67^{+0.12}_{-0.15}$ |
| $EM_1$ ($10^{53}$ cm$^{-3}$) | $5.9 \pm 1.0$ | $2.7^{+1.6}_{-1.3}$ | $2.15^{+1.4}_{-0.6}$ | $4.4^{+2.9}_{-2.4}$ | $5.0^{+5.0}_{-2.7}$ | $4.6^{+1.9}_{-1.7}$ | $3.7^{+5.1}_{-2.9}$ |
| $kT_2$ (keV) | 2.5 (>1.8) | 2.3 (>1.1) | $2.4^{+0.9}_{-0.4}$ | 4.0 (>1.4) | 2.0 (>1.4) | 2.0 (>1.15) | 2.0 |
| $EM_2$ ($10^{53}$ cm$^{-3}$) | $5.2 \pm 0.6$ | $1.5^{+0.9}_{-0.6}$ | $14.8^{+0.5}_{-0.8}$ | $3.8^{+1.7}_{-0.9}$ | $8.5^{+1.0}_{-1.2}$ | $1.7^{+0.7}_{-0.9}$ | 1.5 (<3.3) |
| Abundance ($Z$) | $0.25 \pm 0.04$ | $0.13^{+0.10}_{-0.06}$ | $0.27^{+0.07}_{-0.07}$ | $0.17^{+0.17}_{-0.08}$ | $0.41^{+0.17}_{-0.14}$ | $0.22^{+0.11}_{-0.06}$ | $0.31^{+0.74}_{-0.19}$ |
| $N_H$ ($10^{19}$ cm$^{-2}$) | $3.7 \pm 0.8$ | $4.5^{+3.5}_{-3.2}$ | 0.1 (<1.1) | $6.0^{+3.9}_{-3.9}$ | $6.1^{+1.9}_{-1.8}$ | $23^{+3.5}_{-3.9}$ | $8.1^{+9.0}_{-7.5}$ |
| $\chi^2_\nu$ | 0.91 | 1.47 | 0.62 | 0.70 | 1.13 | 0.96 | 0.79 |

NOTE.—Errors and limits are with 90% confidence for single parameter ($\chi^2_{min} + 2.71$).

[a] One-component fit with $kT \sim 0.8$ keV is also acceptable.

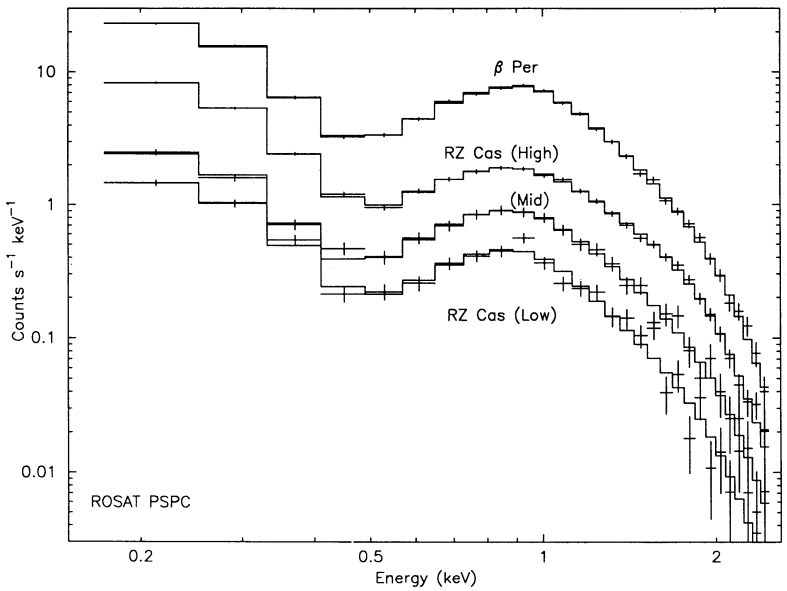


FIG. 5.—X-ray spectra of $\beta$ Per and RZ Cas in its three different states. The best-fit models are shown as the histograms.

7 for $\delta$ Lib and TW Dra. These figures show the "excellent" quality of spectra in the case of $\beta$ Per and RZ Cas in its high state, "very good" to "good" quality of the spectra in the rest of the observations, and the good quality of the fit in all cases.

The CEM plasma models again gave unacceptable fits to the data as compared to the two-component plasma fits above. Such models with solar photospheric abundances resulted in a $\chi^2_\nu \simeq 2$–10 in all cases except TW Dra. For the variable elemental abundances, the values of $\chi^2_\nu$ were 2.28 ($\beta$ Per), 4.10 (RZ Cas "high"), 1.75 (RZ Cas "low"), 0.75 (RZ Cas "mid-"), 3.40 (U Cep), 2.50 ($\delta$ Lib), and 0.90 (TW Dra).

The PSPC spectra are also useful for estimating the absorption column densities toward the stars. It is found, however, that due to the low spectral resolution such estimates are correlated with the estimate of the abundance of the plasma. We illustrate this effect in Figure 8 where we have plotted the 68%, 90%, and 99% confidence contours for the allowed ranges of the abundance and $N_H$ in the case of $\delta$ Lib which has a well-exposed spectrum and significant amount of absorption. Despite this observed correlation, the inferred $N_H$ is generally accurate to about a factor of 2 and does not influence the interpretation given in § 4.3.

#### 3.3.4. *PSPC Spectra: Analysis of RZ Cas and β Per Based on ASCA Results*

The abundances for many elements are better constrained in the *ASCA* spectra, and we have tried using the *ASCA*-determined values for the abundances and the temperatures to constrain the PSPC fits. Allowing only the emission measures and absorption columns to vary, we find that two components

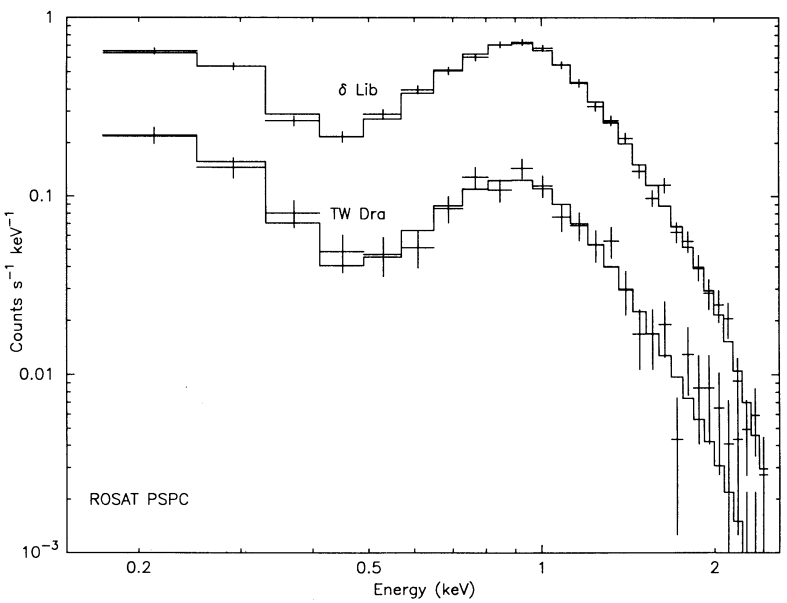


FIG. 6.—X-ray spectra of U Cep in its two different states. The best-fit models are shown as the histograms.

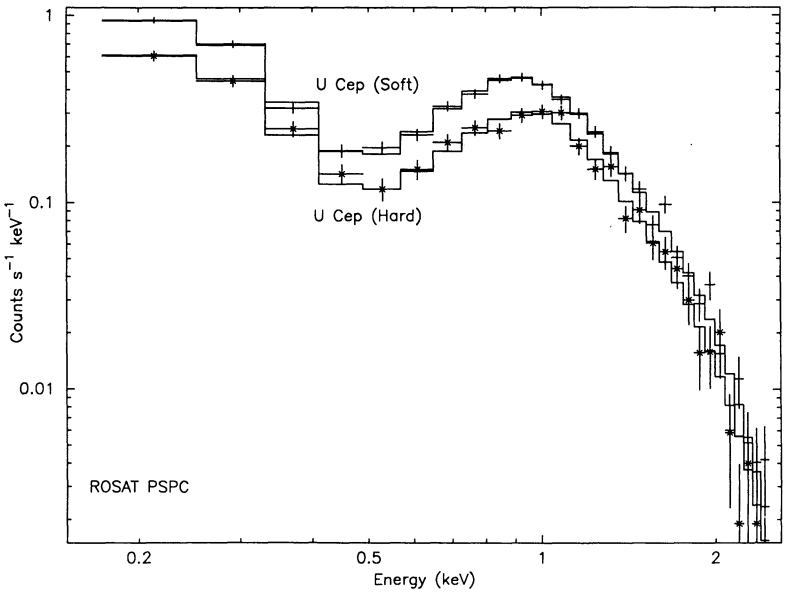


FIG. 7.—X-ray spectra of $\delta$ Lib and TW Dra. The best-fit models are shown as the histograms.

are not adequate for fitting the PSPC spectra of $\beta$ Per and RZ Cas, the $\chi^2_\nu$ being 7.0 for $\beta$ Per, 2.7 for RZ Cas (high state) and 2.1 for RZ Cas (low state). An acceptable fit was obtained to the RZ Cas (mid-state) spectrum with $\chi^2_\nu = 0.9$. The residuals obtained from such a fit to the best quality spectra of $\beta$ Per and RZ Cas (high state) are shown in the top panels of Figures 9*a* and 9*b*. These residuals indicate the presence of a third low-temperature component. Adding a third temperature component with solar abundances and keeping the other two components at the *ASCA*-determined values resulted in an excellent fit to the data on RZ Cas and $\beta$ Per (Table 6). The crude energy resolution of the PSPC, particularly at low energies, does not allow an unambiguous estimate of the abundances for the lowest temperature component. The data can be equally well fitted, albeit with some redistribution of emission measures among the three components, when a third component having the same nonsolar abundances as the other two is added. The EM of the third component with a temperature of 0.2–0.4 keV is only 7%–27% (RZ Cas), and 13% ($\beta$ Per), of the EM of the 0.7 keV component. The *ASCA* spectrum of RZ Cas is not sensitive to the presence of a low-temperature component because of the $\sim$0.4 keV low-energy cut-off of the detectors.

### 3.3.5. *Spectral Variability in U Cep*

A degree of spectral variability seems to be indicated in U Cep (see § 3.2.2). This variability is examined in further detail here. Spectral information was extracted separately for the duration of the "soft" and "hard" states (see Fig. 6). First, we analyzed these spectral data assuming that the temperatures of

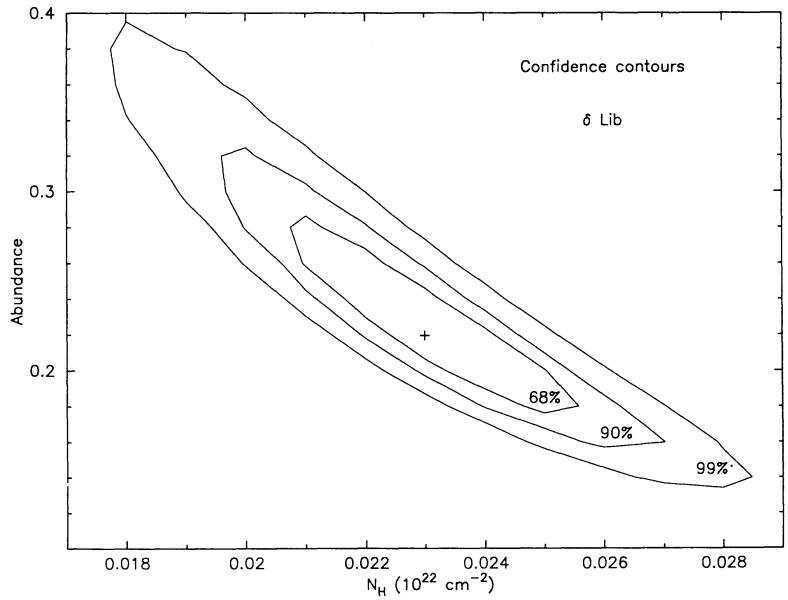


FIG. 8.—Contour plot for the 68%, 90%, and 99% confidence ranges for the absorption column density and abundance parameters in the case of $\delta$ Lib

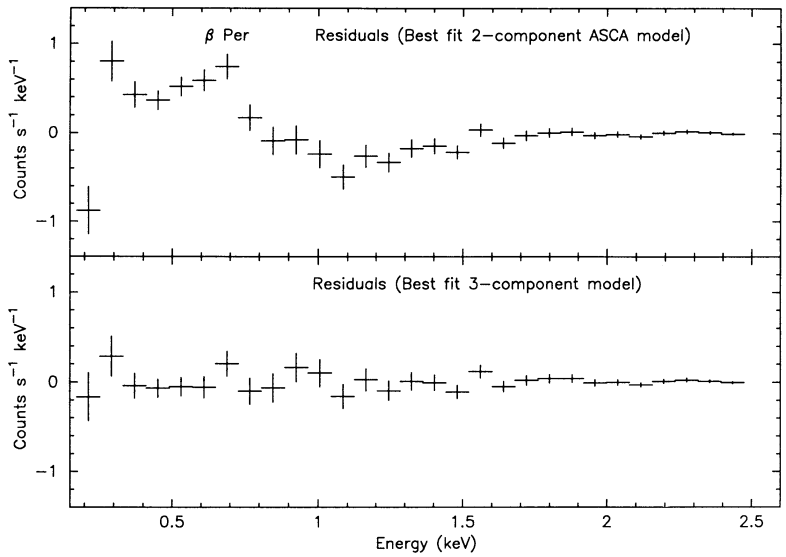


FIG. 9*a*

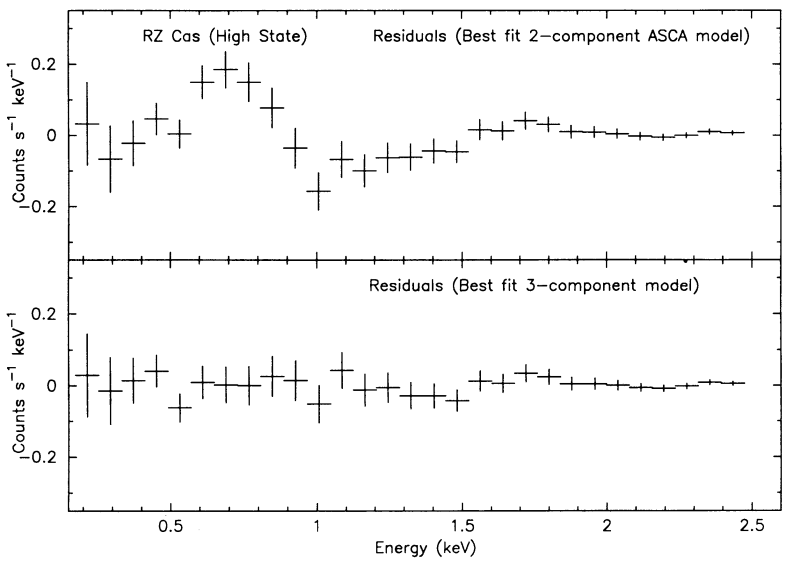


FIG. 9*b*

FIG. 9.—(*a*) Residuals from fits to the *ROSAT* PSPC spectrum of $\beta$ Per based on (i) the best-fit two-component *ASCA* model (*top panel*), and (ii) with the addition of a third temperature component to the *ASCA* model (*bottom panel*). (*b*) Same as in (*a*) for RZ Cas in "high" state.

the two components and elemental abundances obtained from the average spectrum (Table 5) are not changing. A good fit was found for both the spectra ($\chi^2_\nu = 1.05$ for the "soft" state and 1.07 for the "hard" state, for 26 degrees of freedom) that indicated that the change between the two sets of data was entirely due to a change in the emission measure of the low-temperature component. Second, we allowed the temperature of the low-temperature component to vary. An improved fit ($\chi^2_\nu = 0.95$; $\Delta\chi^2 = 4$) was obtained for the "hard" spectrum for a temperature of $0.78 \pm 0.06$ keV with little change in the emission measures, justifying the use of the term "hard" state. There was no change in the fit to the "soft" state spectrum, however, as the temperature of $0.64 \pm 0.04$ keV is very close to the average temperature used earlier. The $N_H$ value was found to be the same in both cases, thus ruling out absorption effects as the cause of the observed hardness ratio variations. Since a third very low temperature ($\sim$0.2 keV) component might be present as indicated in RZ Cas and $\beta$ Per (§ 3.3.4), the possibility of the increased X-ray emission in the "soft" state being due entirely to an increase in the emission of this very soft component in U Cep, cannot be ruled out due to the limited spectral resolution of the PSPC.

## 4. DISCUSSION

The *ASCA* and the PSPC spectra of RZ Cas and $\beta$ Per, and the PSPC spectra of U Cep, $\delta$ Lib, and TW Dra are best fitted by two-component plasma emission models with temperatures of 0.6–0.7 keV and 2–3 keV, and having subsolar abundances (see Tables 3 and 5). The temperatures and the abundances so derived are in excellent agreement. Previous studies (Ottmann 1994; Wade, Stringfellow, & Polidan 1994), however, found that two-component plasma models with solar photospheric

TABLE 6

SPECTRAL RESULTS BASED ON *ASCA*-DETERMINED ABUNDANCES: THREE-TEMPERATURE FITS TO PSPC DATA

| PARAMETER | RZ CAS | | | $\beta$ PER |
|---|---|---|---|---|
| | LOW | HIGH | MID | |
| $kT_1$ (keV) | 2.0 | 2.0 | 2.0 | 2.70 |
| $EM_1$ ($10^{53}$ cm$^{-3}$) | $1.0^{+0.7}_{-0.6}$ | $13.9^{+1.0}_{-1.1}$ | $3.8^{+1.8}_{-1.1}$ | $5.3 \pm 0.3$ |
| $kT_2$ (keV) | 0.7 | 0.7 | 0.7 | 0.64 |
| $EM_2$ ($10^{53}$ cm$^{-3}$) | $1.7^{+0.65}_{-0.90}$ | $1.6^{+1.2}_{-0.9}$ | $2.5 \pm 1.4$ | $3.1 \pm 0.2$ |
| $kT_3$ (keV) | $0.23^{+0.14}_{-0.07}$ | $0.34^{+0.05}_{-0.06}$ | $0.31^{+0.26}_{-0.15}$ | $0.18 \pm 0.014$ |
| $EM_3$ ($10^{53}$ cm$^{-3}$) | $0.14^{+0.10}_{-0.06}$ | $0.44^{+0.08}_{-0.10}$ | $0.18 \pm 0.10$ | $0.41^{+0.09}_{-0.07}$ |
| $N_H$ ($10^{19}$ cm$^{-2}$) | $1.8^{+3.5}_{-1.8}$ | $<0.40$ | $4.2^{+3.5}_{-2.8}$ | $3.1^{+0.9}_{-0.9}$ |
| $\chi^2_\nu$ | 1.55 | 0.68 | 0.68 | 0.88 |

NOTES.—(1) The abundances and $kT$'s of the first two components were fixed from the *ASCA* data (see Table 3 for RZ Cas and Antunes et al. 1994 for $\beta$ Per. (2) The third component with the lowest $kT$ was assumed to have solar composition. (3) Errors are with 90% confidence based on $\chi^2_{min} + 2.71$.

abundances were sufficient for fitting their low signal-to-noise ratio PSPC spectral data. In an analysis of the PSPC spectra of $\beta$ Per using two-temperature plasma emission models assuming solar photospheric abundances, Ottmann (1994) found the two temperatures to be $\sim$0.2 keV and $\sim$1.4 keV, both of which are low when compared to the results from the Solid State Spectrometer (SSS) on the *Einstein Observatory* (Swank et al. 1981), and *ASCA* (Antunes et al. 1994). A similar result can indeed be obtained from the PSPC data presented here but is rejected as it leads to $\chi^2_\nu = 9$. The exposure times used by Ottmann (1994) and Wade et al. (1994) resulted in spectra with low signal-to-noise ratio, which are thus not particularly sensitive to the abundances in the plasma. The low temperatures obtained by Ottmann (1994) compared to our analysis are, therefore, a result of the abundance being constrained to solar photospheric values. This effect was earlier pointed out by White et al. (1994) in the context of an analysis of the coronal spectrum of the RS CVn binary, AR Lac.

We also find that, if we assume that the *ASCA*-determined abundances for the various elements and temperatures of the two plasma components (which are indeed found to be stable) do not change with time, then the PSPC spectra of RZ Cas and $\beta$ Per are best fitted by a three-component plasma model with temperatures of 0.2–0.3 keV ($10^{6.3}$–$10^{6.5}$ K), 0.6–0.7 keV ($\sim 10^{6.9}$ K), and 2–3 keV ($\sim 10^{7.4}$ K), respectively (see Table 6). The third component, however, becomes necessary only under the assumptions mentioned above. The temperature of the very soft component is very similar to that seen as one of the two components in the less active, single late-type stars studied with *ASCA* (Drake et al. 1994). The bulk of the solar corona is also observed to be at this temperature. This suggests the possibility that coronal plasma may have preferred temperatures, regardless of the activity level or the spectral type of the star. This is further discussed in § 4.2. This three-component model is, therefore, an alternative to the successful two-component derived independently from the *ASCA* and the PSPC spectra. It should be possible to detect the very soft component more unambigiously, once the abundances are known individually from high-resolution observations and low-energy high-sensitivity observations are also carried out simultaneously thus increasing the bandwidth of the observations. A joint *EUVE*/PSPC/*ASCA* analysis of these and similar systems will help to constrain very soft plasma component ($T \sim 10^{5.4}$–$10^{6.4}$ K) better.

### 4.1. *Subsolar Elemental Abundances*

The *ASCA* observations have revealed that the line emission from most elements of the coronal X-ray emission of RZ Cas is much less than that predicted for plasmas with solar photospheric abundances, according to the current plasma codes. In order to obtain reasonable fits to these X-ray spectra, the coronal abundances of N, O, Ne, Mg, Si, S, and Fe are required to be about 2–5 times smaller than their values in the solar photosphere. A similar result has been obtained from an analysis of *ASCA* observations of $\beta$ Per by Antunes et al. (1994). Similar subsolar abundances are also implied by the independent analysis of the *ROSAT* PSPC observations of $\beta$ Per, RZ Cas, U Cep, $\delta$ Lib, and TW Dra (see Table 5). A comparison of the coronal abundances in RZ Cas and $\beta$ Per (see Table 3) shows that except for Ne the values of the abundances are nearly identical in the two binaries. The abundance of Ne is, however, subject to the deficiencies in the atomic physics built into the plasma code for the complex of Fe L-shell lines close to the Ne K lines (Liedahl, Osterheld, & Goldstein 1995). The nondetection of Fe K emission in RZ Cas, implies that the inferred abundances of most elements are sensitive to the relative abundance of Fe derived from the Fe L-shell lines.

A general depression of the elemental abundances, compared to their values in the solar photosphere, seems to be present in the coronal X-ray emission of a variety of active late-type stars: RS CVn binary AR Lac (White et al. 1994), the quiescent emission from flare stars (Gotthelf, Mukai, & White 1994), and to a lesser extent even active single G/K-type stars (Drake et al. 1994). The similarity of the coronal abundance values in the two Algol binaries RZ Cas and $\beta$ Per with those of the RS CVn binary AR Lac is quite remarkable. In contrast, in single late-type stars the abundances of Mg, Si, and Fe are closer to the solar photospheric values (Drake et al. 1994), suggesting that the magnitude of the abundance anomaly is correlated with activity level.

The coronal abundances in the active regions of the Sun are known to be quite different from the photospheric abundances and to exhibit the so-called FIP (First Ionization Potential) effect, in that the abundances of those elements such as Fe, Si,

and Mg having first ionization potentials less than $\sim 10$ eV are enhanced by typically a factor of 4 compared to those elements like H and O with higher FIP values (Meyer 1985; Waljeski et al. 1994). There is no clear evidence for such a pattern in the two single G stars studied with *ASCA* by Drake et al. (1994). The FIP effect is also absent in the *ASCA* spectra of RS CVn binary AR Lac (White et al. 1994), $\beta$ Per (Antunes et al. 1994) and RZ Cas (present study), and dMe stars (Gotthelf et al. 1994), and in the EUVE spectrum of the F5 IV–V star Procyon (Drake, Laming, & Widing 1995). Thus, an underabundance of most elements seems to be prevalent in a variety of highly active coronal X-ray sources.

The fact that the elemental abundances are nonsolar affects the conversion of counts to flux and also the relative values of the EM of the two-temperature components: almost all previous estimates of the conversion factor for the PSPC count rates of coronal sources have assumed solar abundances. Our analysis shows that the conversion factor for coronal sources like Algols, is $\sim 8.5$–$9.0 \times 10^{-12}$ ergs cm$^{-2}$ count$^{-1}$ s$^{-1}$, as compared to the value of $6 \times 10^{-12}$ ergs cm$^{-2}$ count$^{-1}$ s$^{-1}$ used by Dempsey et al. (1993a, b) assuming solar abundances. The EM of the low-$T$ component goes up for subsolar abundances and becomes almost comparable to the EM of the high-$T$ component, as can be seen from Figure 4. These effects can influence the statistical correlations among various parameters derived for a larger sample of such objects, for example, in the case of a sample of RS CVn's studied by Dempsey et al. (1993b).

### 4.2. *Discrete Component Coronal Emission versus CEM*

We find that discrete (two- or three-) component plasma emission models can usually better fit the data than the power-law CEM models based on models of single solar loops; the latter models are even found to be unacceptable in several cases. The reality of the discreteness of the EM distribution is further confirmed when we derive very narrow widths for the assumed Gaussian distributions of EM centered on discrete values of temperatures. A similar result has been reported earlier by Dempsey et al. (1993b) for the RS CVn binaries, and Lemen et al. (1989) had also argued in favor of a discrete component model based on high-resolution data (*EXOSAT* Transmission Grating) of Capella, Procyon and an RS CVn binary ($\sigma^2$ CrB). According to Lemen et al. (1989) the discrete components represent the distinct ensemble of static loops with different maximum temperatures and expansions of the loop cross section from the footpoint to the apex.

The two or three temperatures dominating the X-ray spectrum of RZ Cas and $\beta$ Per (and perhaps all the Algols) correspond to the regions of shallow positive gradients in the plasma cooling curve and, in fact, do avoid the regions of steep negative slopes. This was first pointed out, mainly in the context of the two-temperature components, by Lemen et al. (1989) and later elaborated upon by Gehrels & Williams (1993). The significance of this result is that the dominant temperatures are those where the coronal plasma is stable to thermal fluctuations. The exact regions of preferred temperatures may, however, vary from object to object depending on the heating mechanisms and the abundances of elements in the plasma which affect the cooling curve. A detailed investigation of discrete component models versus CEM models for stellar coronae, based on high-quality spectral observations of AR Lac, an RS CVn binary, carried out simultaneously with *ROSAT* and *ASCA* will be presented elsewhere (Singh et al. 1995).

### 4.3. *Low-Energy Absorption in Algols*

The low-energy response of the PSPC and a proper modeling of the emission continuum allows us to obtain a measure of the absorption and thus the presence of cold circumstellar matter within these Algol binaries. We, however, wish to stress that because of the low spectral resolution of the PSPC the determination of absorption column is correlated with the determination of abundance in the plasma as already pointed out in § 3.3.3 and illustrated in the case of $\delta$ Lib. Using the data for the stars closer than 200 pc from Paresce (1984) and assuming that for more distant or high-latitude stars, the $N_{\rm H}$ is about 50% of the total Galactic column density estimated from 21 cm surveys (e.g., Stark et al. 1992), we can estimate the maximum expected column density toward the stars. This gives values of 1.0, 7.0, 70, 10, and $10 \times 10^{19}$ cm$^{-2}$ for $\beta$ Per, RZ Cas, U Cep, $\delta$ Lib, and TW Dra, respectively. Another way to estimate the column densities toward these stars is to assume a uniform density of 0.07 cm$^{-3}$ derived for the solar neighborhood by Paresce (1984); this results in values of 0.7, 1.6, 3.7, 1.6, and $4.1 \times 10^{19}$ cm$^{-2}$ for $\beta$ Per, RZ Cas, U Cep, $\delta$ Lib, and TW Dra, respectively. For a third estimate of the $N_{\rm H}$ we can use the recent compilations by Fruscione et al. (1994) and Diplas & Savage (1994) that are mostly based on *IUE* observations of stars: for each Algol we infer $N_H$ based on the tabulated column densities for the 10 nearest stars to them (in three-dimensional space) and get values of 0.25, 2.5 and $2.4 \times 10^{19}$ cm$^{-2}$ for $\beta$ Per, RZ Cas, and $\delta$ Lib, respectively. There are not enough nearby stars with measured $N_{\rm H}$ values for us to use this method for U Cep and TW Dra. The latter two estimation techniques are likely to yield lower limits on $N_{\rm H}$.

A comparison of the above estimates for $N_{\rm H}$ with the best-fit values listed in Tables 5 and 6 shows that there may be an excess absorption due to circumstellar material in $\beta$ Per and $\delta$ Lib. In the PSPC observation of RZ Cas when in its high state, we have inferred a column density that is significantly lower than that expected for this star; this is due perhaps to the presence of unresolved soft emission. The other X-ray–derived values of $N_{\rm H}$ in RZ Cas (Tables 5 and 6) seem to be consistent with the estimates from UV and radio data quoted above. There is only marginal evidence for excess absorption in one of the observations of RZ Cas—its "mid-" state which is close to its primary eclipse. A simultaneous EUVE/X-ray observation of this system is needed to discern between a variable column density toward RZ Cas, which might be related to the transient optical absorption features that have been noted in similar binaries, or a variable soft excess.

The presence of circumstellar matter due to transient disks surrounding the primary star and in the region between the two stars in $\beta$ Per has been shown by Richards (1993). The presence of X-ray absorption in the present observations close to the primary eclipse would imply that the matter is distributed extensively around the binary system. The results for $\delta$ Lib imply an extremely high absorption which should be quite easy to confirm with further observations. So far there are no reports of optical absorption in $\delta$ Lib. It is also worth pointing out, that the primary in $\delta$ Lib is very massive for its spectral type and that extensive mass transfer seems to have taken place in this system, a fact pointed out quite early on (Tomkin 1978).

### 4.4. *X-Ray Variability*

The X-ray light curve of RZ Cas shows a factor of ~3 variability. In the PSPC observations, the system goes from a "low" state to a "high" state and is subsequently caught in a "mid-" state. The spectral analysis shows that this activity is mostly related to variations in the emission measure of the high-temperature (2–3 keV) component. In the absence of having observed either the rise or decline of the intensity, it is not clear whether these variations are due to flares or due to rotation of active regions on the surface of the active star. Since the temperature might be expected to increase significantly during a flare (White et al. 1986; Stern et al. 1992), the observed constancy of the temperatures of the two components in the corona of RZ Cas favors a rotational modulation interpretation (but the temperature of the high-temperature component is only weakly constrained by the PSPC due to its soft bandpass).

X-ray emission from U Cep was observed to decrease over a timescale of one-half a day: again, it is impossible to distinguish whether this was due to the slow decay of a long-duration flare or to the rotational modulation of an active region as it moves toward the limb as the cause for these variations. These observations further suggest that excess X-ray emission originates from cooler coronal loops closer to the surface of the star whereas the lowest level of emission comes from larger and hotter loops.

The X-ray light curve of $\beta$ Per has recently been found to be quite stable over a few binary periods (Ottmann 1994), and over months and possibly a few years (Antunes et al. 1994). The present observations further support this finding (see § 3.2.3) and thus strengthen the view that the rotation modulation of the active regions on the late-type star is responsible for the quiescent X-ray light curve. The *ROSAT* observations imply a compact or sharp trailing edge for the coronally active regions near phase 0.08.

## 5. CONCLUSIONS

In conclusion, the present study of X-ray emission from Algols finds that (*a*) the coronal X-ray emission from these systems is composed of at least two discrete components of plasma with temperatures of 0.6–0.7 keV and 2–3 keV, (*b*) a third component with a temperature of 0.2–0.3 keV component may be present in some systems, (*c*) the elemental abundances are one-fifth to one-half of the solar photospheric values, (*d*) excess circumstellar or circumbinary low-energy absorption is not very common but may be present in some systems like $\delta$ Lib and $\beta$ Per, (*e*) RZ Cas shows variable X-ray emission and exhibits a "low," "high," and "mid-" state of activity strongly associated with the changes in the emission measure of the high-temperature (2–3 keV) component and mildly associated with changes in the softer component, (*f*) U Cep shows an increased X-ray emission associated with the softer temperature (0.6–0.7 keV) component, and (*g*) $\beta$ Per exhibits a very stable feature in its light curve making it highly asymmetric. We have presented some preliminary interpretations of these observed properties of the coronae of Algol binary stars. Before a more detailed analysis is warranted, we believe that there is a crucial need for improved theoretical coronal plasma models that include the recent corrections to the Fe L-shell complex (Liedahl et al. 1994). More extended X-ray observations of selected Algol binaries that cover one or more orbital periods would also be extremely helpful in enabling us to discriminate between stochastic variability such as flaring and rotational modulation of active regions as the causes for the observed X-ray variability of these stars.

We thank the entire *ASCA* and *ROSAT* teams for making these observations possible. We thank an anonymous referee for her or his comments and suggestions. This research has made use of the Simbad database, operated at CDS, Strasbourg, France.

## REFERENCES

Anders, E., & Grevesse, N. 1989, Geochim. Cosmochim. Acta, 53, 197
Antiochos, S. K., & Noci, G. 1986, ApJ, 301, 440
Antunes, A., Nagase, F., & White, N. E. 1994, ApJ, 436, L83
Day, C. S. R., et al. 1994, The ABC Guide to *ASCA* Data Reduction, *ASCA* Guest Observer Facility, NASA/Goddard Space Flight Center
Dempsey, R. C., Linsky, J. L., Fleming, T. A., & Schmitt, J. H. M. M. 1993a, ApJS, 86, 599
Dempsey, R. C., Linsky, J. L., Schmitt, J. H. M. M., & Fleming, T. A. 1993b, ApJ, 413, 333
Diplas, A., & Savage, B. D. 1994, ApJS, 93, 211
Drake, J. J., Laming, J. M., & Widing, K. G. 1995, ApJ, 443, 393
Drake, S. A., Singh, K. P., White, N. E., & Simon, T. 1994, ApJ, 436, L87
Faulkner, D. R. 1986, PASP, 98, 690
Fruscione, A., Hawkins, I., Jelinsky, P., & Wiercigroch, A. 1994, ApJS, 94, 127
Gehrels, N., & Williams, E. D. 1993, ApJ, 418, L25
Giuricin, G., Mardirossian, F., & Mezzetti, M. 1983, ApJS, 52, 35
Gotthelf, E. V., Mukai, K., & White, N. E. 1994, ApJ, 1994, submitted
Grevesse, N., Noels, A., & Sauval, N. J. 1992, in Proc. of the First SOHO Workshop (ESA SP-348) (Noordwijk: ESA Publication Division, ESTEC), 305
Hall, D. S. 1989, Space Sci. Rev., 50, 219
Kaastra, J. S. 1992, An X-Ray Spectral Code for Optically Thin Plasmas (SRON-Leiden Report, updated version 2.0)
Kim, H. 1989, ApJ, 342, 1061
Lemen, J. R., Mewe, R., Schrijver, C. J., & Fludra, A. 1989, ApJ, 341, 474
Liedahl, D. A., Osterheld, A. L., & Goldstein, W. H. 1995, ApJ, 438, L115
McCluskey, G. E., Jr., & Kondo, Y. 1984, PASP, 96, 817
Mewe, R., Gronenschild, E. H. B. M., & van den Oord, G. H. J. 1985, A&A, 62, 197
Meyer, J.-P. 1985, ApJS, 57, 173
Narusawa, S., Nakamura, Y., & Yamasaki, A. 1994, AJ, 107, 1141
Ottmann, R. 1994, A&A, 286, L27
Paresce, F. 1984, AJ, 89, 1022
Pfeffermann, E., et al. 1987, Proc. SPIE, 733, 519
Raymond, J. C. 1990, private communication
Raymond, J. C., & Smith, B. W. 1978, ApJS, 35, 419
Richards, M. T. 1993, ApJS, 86, 255
Richards, M. T., & Albright, G. E. 1993, ApJS, 88, 199
Schmitt, J. H. M. M., Collura, A., Sciortino, S., Vaiana, G. S., Harnden, F. R. Jr., & Rosner, R. 1990, ApJ, 365, 704
Singh, K. P., et al. 1995, in preparation
Smale, A., et al. 1995, in preparation
Stark, A. A., Gammie, C. F., Wilson, R. W., Bally, J., Linke, R. A., Heiles, C., & Hurwitz, M. 1992, ApJS, 79, 77
Stern, R. A., Antiochos, S. K., & Harnden, F. R. 1986, ApJ, 305, 417
Stern, R. A., Uchida, Y., Tsuneta, S., & Nagase, F. 1992, ApJ, 400, 321
Swank, J. H., White, N. E., Holt, S. S., & Becker, R. H. 1981, ApJ, 246, 208
Tanaka, Y., et al. 1994, PASJ, 46, L37
Tananbaum, H., et al. 1979, ApJ, 234, L9
Tomkin, J. 1978, ApJ, 221, 608
Truemper, J. 1983, Adv. Space Res., 2, 241
Turner, T. J., & George, I. M. 1994, "*ROSAT* PSPC Calibration Guide" (documentation available at US *ROSAT* Science Data Center & HEASARC)
Vesecky, J. F., Antiochos, S. K., & Underwood, J. H. 1979, ApJ, 233, 987
Wade, R. A., Stringfellow, G., & Polidan, R. S. 1994, preprint
Waljeski, K., Moses, D., Dere, K. P., Saba, J. L., Strong, K. T., Webb, D. F., & Zarro, D. M. 1994, ApJ, 429, 909
White, N. E., et al. 1994, PASJ, 46, L97
White, N. E., Culhane, J. L., Parmar, A. N., Kellett, B. J., Kahn, S., van den Oord, G. H. J., & Kuijpers, J. 1986, ApJ, 301, 262
White, N. E., & Marshall, F. E. 1983, ApJ, 268, L117